coatings

MDPI

Article

Experimental Study on Pipeline–Soil Interaction in Translational Landslide

Tianjun Xue [1], Lingxin Liu [1], Jianlei Zhang [1,2,*], Mengjie Dai [1], Gengyuan Shi [1] and Xinze Li [1]

[1] China University of Petroleum (Beijing) at Karamay, Karamay 834000, China; 2023015296@st.cupk.edu.cn (T.X.); 2022016291@st.cupk.edu.cn (L.L.); 2023216912@st.cupk.edu.cn (M.D.); 2022216845@st.cupk.edu.cn (G.S.); lixinze@cupk.edu.cn (X.L.)
[2] Xinjiang Key Laboratory of Multi-Medium Pipeline Safety Transportation, Urumqi 830011, China
* Correspondence: zhangjianlei@cupk.edu.cn

Abstract: Pipelines in landslide-prone areas are highly susceptible to damage or rupture under soil movement, posing severe threats to social stability and national security. However, research on pipeline failure mechanisms across different landslide types remains insufficient. Therefore, this study employs large-scale indoor model tests to investigate the interaction mechanisms between pipelines and soil (pipeline–soil interaction) in translational landslide zones through comparative experiments. The results indicate that: (1) The failure process of translational landslides is characterized by initial sliding at the slope crest under loading, which progressively drives the lower soil mass, ultimately resulting in global slope instability. The sliding mass displacement exhibits a top-to-bottom reduction pattern. (2) Pipelines traversing slopes laterally significantly enhance slope stability by providing measurable anti-sliding resistance. (3) Pipeline displacement under sliding mass action occurs in the downslope direction, yet its trajectory deviates from the sliding mass movement. (4) Strain analysis reveals that the pipeline experiences peak strain in the middle region of the sliding mass and at the sliding-non-sliding interface, with the middle region being the primary location for initial yielding and fracture. This study advances the understanding of pipeline-sliding mass interaction mechanisms in translational landslides and offers critical insights for improving pipeline safety and reliability.

Keywords: translational landslide; pipeline; pipeline–soil interaction; model test

Academic Editor: Manuel Miguel Jordan-Vidal

Received: 7 April 2025
Revised: 24 April 2025
Accepted: 28 April 2025
Published: 30 April 2025

Citation: Xue, T.; Liu, L.; Zhang, J.; Dai, M.; Shi, G.; Li, X. Experimental Study on Pipeline–Soil Interaction in Translational Landslide. *Coatings* **2025**, *15*, 537. https://doi.org/10.3390/coatings15050537

1. Introduction

Pipelines serve as a crucial means of transporting oil and gas, playing an irreplaceable strategic role in ensuring social stability and safeguarding national security [1–4]. As a result, pipeline engineering is widely regarded as the lifeline of national energy supply. With the rapid development of pipeline engineering towards large-diameter and long-distance systems, pipelines inevitably traverse complex and varied terrains [5,6]. During the construction of long-distance buried pipelines, geological instability along the routes has become increasingly prominent, potentially triggering multiple geohazards [7,8]. Among these, landslides are one of the most common types of geohazards that pose severe threats to pipeline safety [3,9–11]. Notably, over 96% of pipeline accidents caused by ground movement are attributed to landslide-related disasters [9]. Under the influence of landslides, pipelines may experience local buckling, tensile failure, or rupture due to excessive loads, leading to leaks and subsequent catastrophic incidents such as fires and explosions, which endanger both safety and the environment.

Currently, both domestic and international scholars have conducted experimental research on the interaction between pipelines and soil in landslide-prone areas. These experiments primarily include small-to-medium-scale indoor model tests under 1 g of gravitational acceleration, large-scale outdoor model tests, and centrifuge testing.

Lin et al. [12] conducted indoor experiments to explore the mechanical and deformation characteristics of pipelines subjected to landslides. Their results revealed that the axial stress distribution along the pipeline approximates a saddle-shaped pattern, with stress peaks observed at the center and lateral boundaries of the landslide width, while maximum deformation occurs at the center of the landslide width. Feng et al. [13] performed a large-scale outdoor test to study the deformation and failure mechanisms of slopes, specifically examining the transition from continuous sliding to shallow drift sliding occurring above the pipeline, as well as the deep compressive deformation occurring beneath it. The findings indicate that the presence of the pipeline contributes to improved slope stability by redistributing deformation towards the peripheries and mitigating the maximum displacement in the direction of the landslide.

To investigate the degradation of soil strength induced by water infiltration, several researchers have incorporated permeation or simulated rainfall systems into their experiments. For instance, Calvetti et al. [14] conducted small-scale 1 g model tests by decomposing relative displacement and tensile forces into horizontal and vertical components to analyze plane strain and loading states during pipeline–soil interaction. By horizontally pulling the pipeline under seepage conditions and varying pipeline diameters and burial depths, they identified critical characteristics of pipe–soil interaction and displacement patterns. Lian et al. [15] developed an indoor slope instability model to study rainfall-induced interactions between buried gas pipelines and soil, building on flume experiments. By monitoring sectional strain in pipelines during rainfall-induced slope failure, they quantified the effects of soil on pipeline behavior. Guan et al. [16] investigated the interaction mechanisms and failure evolution of micropile-reinforced landslide-pipeline systems through large-scale indoor physical model tests. Mohammad et al. [17] conducted 10 displacement-controlled pulling tests on a 324 mm-diameter, 6.35 mm-wall-thickness steel pipe segment (2.4 m long) embedded in dense sandy slopes at varying burial depths. They systematically analyzed the effects of embedment ratio and slope inclination on the relationship between lateral soil forces and relative pipeline displacement responses, with comparative evaluations against horizontal ground conditions.

To enhance the accuracy of mechanical analyses for pipelines in landslide zones, centrifuge testing has been adopted by researchers. This method generates body stress gradients that are equivalent to prototype conditions, ensuring similarity in effective stress and pore pressure at corresponding depths. Nasser et al. [18] conducted a series of centrifuge tests to study pipeline–soil interactions under axial, oblique, and lateral loading in dense sand. Zhang et al. [19] induced slope instability through crest loading in 30 g centrifuge tests. They performed experiments on six coarse-grained dense sand slopes with pipelines positioned at various locations relative to the slope crest, as well as on two medium-dense fine sand slopes, to investigate the influence of particle size distribution on pipeline–soil interactions. A novel methodology was proposed for calculating the ultimate external forces acting on buried pipelines at different slope positions during landslide failure.

However, current experimental studies on pipeline–soil interactions in slopes primarily emphasize factors such as pipeline burial depth, crossing configurations, sliding mass volume, and slope inclination. However, there is a notable lack of systematic research regarding the impact of different landslide types. Different landslide classifications

demonstrate different sliding mechanisms that exert diverse effects on pipelines. For example, in the case of translational landslides, the upper sliding mass drives the overall movement of the slope, while the lower slope body provides partial resistance, thereby slowing the progression of the landslide. In contrast, retrogressive landslides originate from the lower sliding mass, which destabilizes the upper slope due to the loss of basal support, consequently accelerating the sliding process. Therefore, this study conducted a series of large-scale indoor tests based on the Xiaozhai Village landslide case. It conducts comparative experiments aimed at elucidating the mechanisms of pipeline–soil interaction during translational landslides. Two distinct experimental setups were implemented: (1) slope instability tests conducted in the absence of pipelines, and (2) slope instability tests that included a PVC pipeline positioned laterally across the slope. The results of this investigation contribute to a deeper understanding of pipeline–soil interactions in the context of translational landslides, thereby offering a theoretical framework for mitigating pipeline hazards in areas susceptible to landslides.

2. Experimental Section

2.1. Experimental Scheme

This study conducted two comparative experimental groups based on the Xiaozhai Village landslide prototype: (1) a slope instability test conducted without the inclusion of pipelines (Experiment-L) and (2) a slope instability test incorporating a PVC pipeline that traverses the slope laterally (Experiment-LP). A comparative analysis of these two experimental groups was performed to systematically examine the impact of pipelines on slope-instability patterns, thereby clarifying the mechanisms of pipeline–soil interaction in the context of translational landslides.

The Xiaozhai Village landslide is located on the right side of the Shazi–Xingren Highway in Qinglong County, Guizhou Province, near the China–Myanmar gas pipeline project. During the construction of the pipeline, a significant amount of excavated soil was deposited alongside the pipeline route, which considerably altered the original slope angle and increased the surcharge load at the slope crest. This disturbance disrupted the natural equilibrium of the slope. Ultimately, the failure of the slope was triggered by external factors, including rainfall, resulting in a landslide event. The landslide caused the gas pipeline to fracture, which subsequently led to leakage and combustion [19].

As illustrated in Figure 1, the landslide spans an elevation range from 1380 m at the toe to 1400 m at the crown, resulting in a relative height differential of 20 m. The predominant direction of sliding is oriented at 80°, with slope angles varying between 30° and 40° (averaging 35°), indicating a profile that is gentle in the upper section and steep in the lower section. The dimensions of the landslide are 40 m in length, 40 m in average width, and a thickness ranging from 4 to 8 m, which corresponds to a total volume of 9.6×10^3 m^3, thereby categorizing it as a small-scale landslide. The sliding mass exhibits an irregular semi-elliptical shape with distinct chair-like contours [20]. The slope is composed of near-horizontal, thin-to-medium-bedded Triassic fine sandstone, which is covered by a thin layer of gravelly soil. A cross-sectional view of the landslide is illustrated in Figure 2.

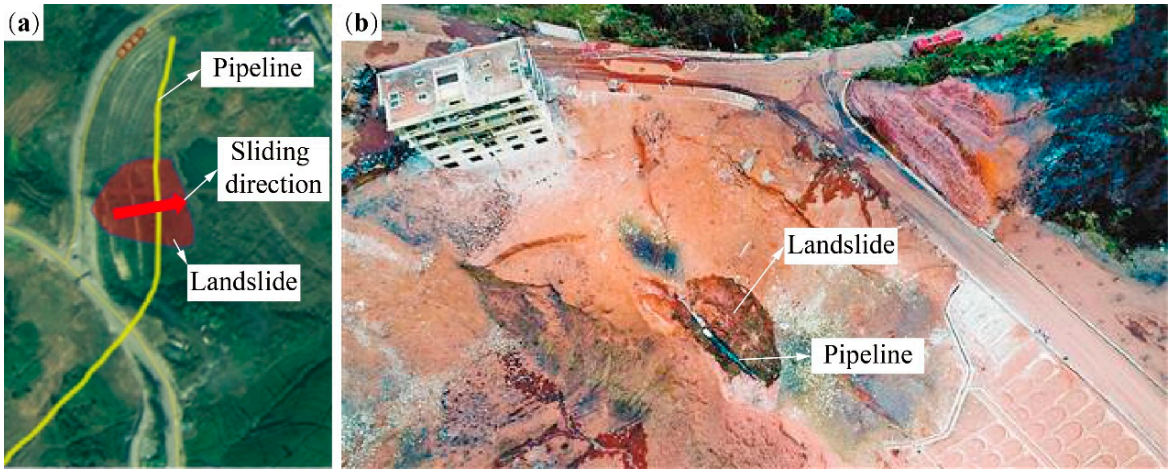

Figure 1. Pipeline–soil interaction in the Xiaozhai Village landslide: (**a**) Pipeline route; (**b**) Pipeline failure caused by landslide.

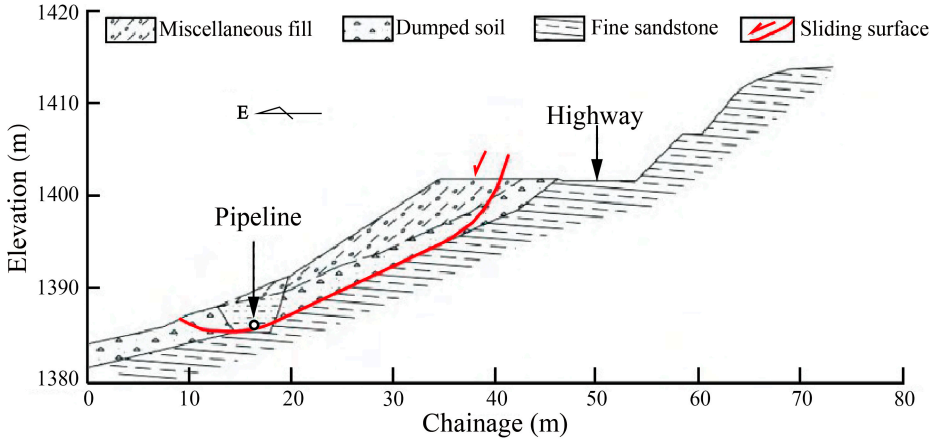

Figure 2. Cross-sectional view of Xiaozhai Village landslide.

2.2. Experimental Material

The soil samples utilized in this study were obtained from the Karamay Campus of China University of Petroleum (Beijing). The soil density was measured at 2142 kg/m^3 using the ring knife method. Shear strength parameters, specifically cohesion (11.59 kPa) and the internal friction angle (25.71°), were measured using an electric direct shear apparatus, as shown in Figure 3. The soil of the Xiaozhai Village landslide has a density of 2100 kg/m^3, cohesion of 10 kPa, and an internal friction angle of 24°. These parameters demonstrate a strong correlation with the in situ shear strength values of the soil from the Xiaozhai Village landslide, thereby confirming the representativeness of the selected soil samples.

The polyvinyl chloride (PVC) pipeline utilized in the experiments had a nominal outer diameter of 30 mm and a wall thickness of 1 mm. The mechanical properties of the pipeline material were characterized as follows: Young's modulus of 2.4 GPa, Poisson's ratio of 0.38, yield strength of 40 MPa, and tensile strength of 50 Mpa. Although there are differences in mechanical properties between PVC pipelines and steel pipelines in the plastic stage, their mechanical properties in the elastic stage are generally consistent. This study mainly focuses on the deformation characteristics and strain distribution of pipelines in the elastic stage. Therefore, although the model has an idealized representation of the landslide and pipeline, this comparative experiment can reveal the mechanism of pipeline–soil interaction.

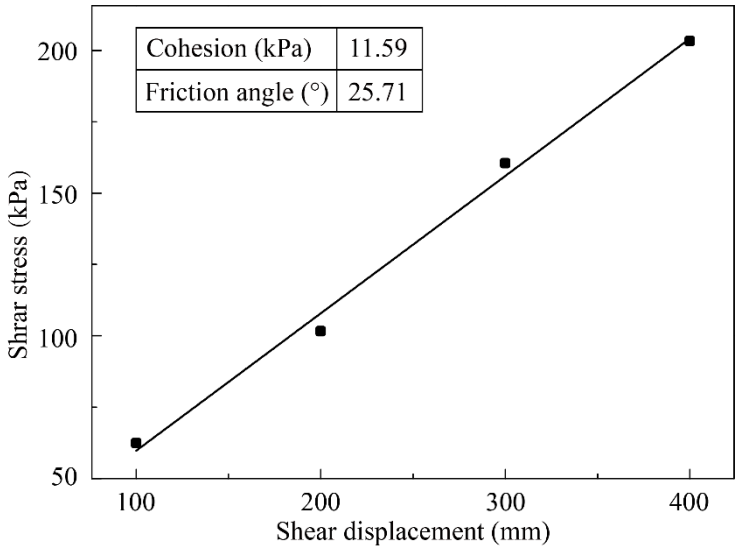

Figure 3. The relationship between the shear stress and shear displacement in the direct shear test.

2.3. Model Construction

2.3.1. Landslide Model Construction

The experimental model is constructed within a model box measuring 2.4 m in length, 1.8 m in width, and 1.5 m in height. The sliding mass in Xiaozhai Village measures 40 m in length, with an average width of approximately 40 m. A 12 m-wide non-sliding region has been established on both sides of the landslide to reduce the impact of boundary constraints on the pipeline. To ensure the accuracy of the experimental results, the geometric similarity ratio was set at 1:30. The other similarity ratios are summarized in Table 1. According to the principle of similarity, the reduced-scale soil box model established for the experiment may exhibit size effects. The geometric scaling of the soil model can affect the sliding displacement rate and crack formation, potentially leading to deviations from the prototype landslide. However, the effect of geometric scaling on the mechanism of pipeline–soil interaction is relatively minor. The model box was constructed with steel plates and tempered glass panels to enable the observation of landslide dynamics. The indoor landslide model comprises four key components: the bedrock, the slip zone, the sliding mass, and the non-sliding regions. The parameters for each component are determined based on the landslide in Xiaozhai Village and the experimental scale, as detailed in Figure 4.

Table 1. Similar parameters.

Physical Parameters	Units	Similitude Relationships	Scaling Ratios
Geometric dimensions	m	C_l	1:30
Gravity	m/s^2	C_g	1:1
Density	Kg/m^3	C_ρ	1:1
Stress	N/m^2	$C_\sigma = C_l C_g C_\rho$	1:30
Strain	/	C_ε	1:1

During the sliding process, the bedrock and non-sliding regions remain in a state of rest. To model this phenomenon, three support walls were constructed using bricks and concrete according to prototype dimensions. Wooden plates with a thickness of 2 cm were affixed to these walls to replicate the characteristics of bedrock (Figure 5). The sliding zone refers to the shear zone that exists between the sliding mass and the stable bedrock beneath it. Consequently, in the modeling process, the slip zone is established at the interface between the bedrock layer and the sliding mass layer. Due to its inherently low shear strength,

characterized by minimal cohesion and a low internal friction angle in relative to the sliding mass [21–23], a plastic film was positioned across the width of the landslide. This film was subsequently covered with a 2 cm-thick layer of sand to create a weak slip zone (Figure 5).

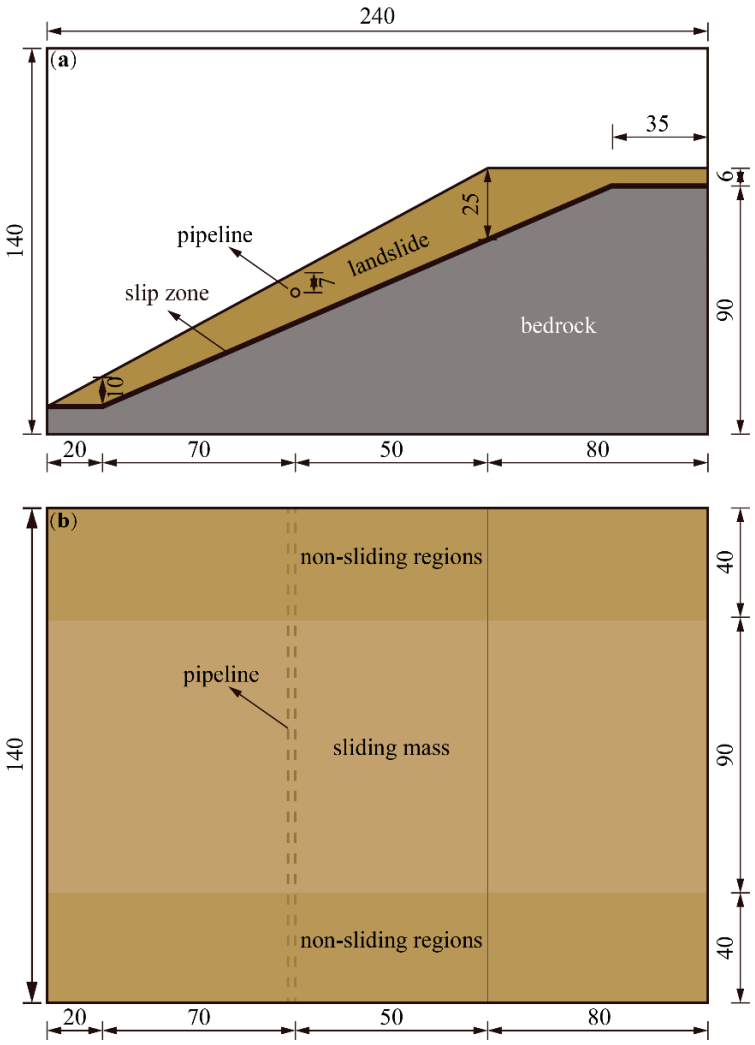

Figure 4. The indoor model test: (**a**) Side view; (**b**) Top view.

The configuration of the sliding mass has been simplified based on the experimental prototype, as illustrated in Figure 4. The sliding mass has a width of 1.2 m and an average thickness of 20 cm, which is segmented into four layers for installation, each with a thickness of 5 cm in the Experiment-L. In accordance with the principles governing the relationship between density and volume, the soil required for each layer is deposited and compacted using compaction tools to replicate the density characteristics of an actual sliding mass. The lengths of the non-sliding regions flanking the model are 0.4 m, with an average thickness of 21 cm, and the installation procedure employed is consistent with that of the sliding mass.

The methodology employed for the Experiment-LP closely resembles that of Experiment-L. The pipeline is installed at a burial depth of 1.8 m within both the sliding mass and the non-sliding regions, according to the experimental prototype. Field investigations indicate that when the length of the pipeline in the non-sliding regions exceeds 9 m, the pipeline remains essentially stationary. Consequently, bricks are positioned approximately 0.3 cm from the sliding mass to establish the boundary of the pipeline in the Experiment-LP. After the installation of the pipeline, the upper layer of the sliding mass is covered to a predetermined thickness. The configuration of the pipeline is illustrated in Figure 5.

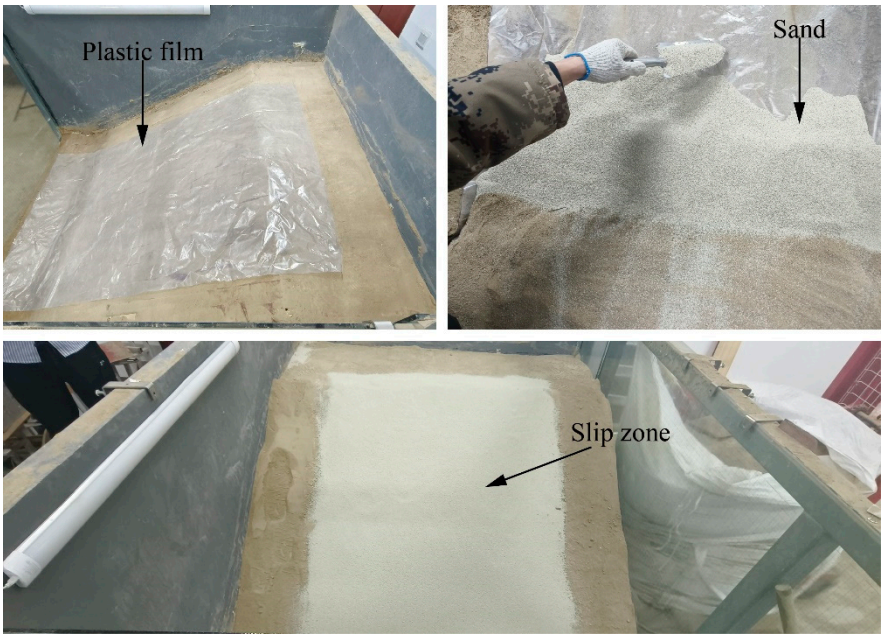

Figure 5. The construction process of the slip zone.

2.3.2. Measurement of Experimental Data

During the experiments, displacements at both the surface and internal positions of the sliding mass, the pipeline displacements, and strain distributions along the pipeline were systematically observed. All electrical signals were recorded using a DH5922D dynamic signal-acquisition system. The DH5922D dynamic signal-acquisition system was employed for parameter monitoring with a measurement accuracy of ±0.1% full-scale range and a sampling rate of 204.8 kHz per channel. This system is capable to monitor the strain by the strain gauges (resistance: 120 ± 0.1 Ω, gauge factor: 2.0 ± 0.1%, strain limit: 2%) and the displacement using the laser-displacement sensors (measuring range: 400 ± 200 mm, repeatability: 400/800 μm, linearity: ±0.2% full scale range).

The surface displacements of the sliding mass were qualitatively recorded using three sand marker strips (Figure 6): one located directly above the pipeline, one positioned diagonally above the pipeline, and one situated diagonally below the pipeline. These strips enabled the visual monitoring of displacement patterns at the landslide surface.

Internal displacements within the sliding mass and the displacements of the pipeline were measured using paired monitoring blocks connected by wires. One block was embedded in the sliding mass, while the corresponding block was mounted on a platform atop the test box. A laser-displacement sensor was utilized to monitor the movements of the block mounted on the platform, thereby facilitating the indirect quantification of internal displacements within the sliding mass and the displacements of the pipeline. The specific configurations of this setup are illustrated in Figure 6.

There are 16 channels in the DH5922D dynamic signal-acquisition system. The laser-displacement sensors require four channels. Four strain gauges are required at each cross-section of the pipeline in the experiment. Every strain gauge needs one channel. Therefore, three cross-sections of the pipeline can be monitored. Three cross-sections exhibiting typical mechanical responses were selected: (a) the mid-span of the pipeline, which tends to exhibit significant mechanical responses; (b) the interface between the sliding mass and the non-sliding regions, which serves as a dynamic-static boundary, also influences the pipeline strain distribution; (c) the cross-section at the midpoint between two aforementioned cross-sections was selected to reveal the strain distribution patterns along the pipeline. Strain gauges were mounted on an identical pipeline prior to experimental testing to

calibrate the strain gauges and the signal-acquisition system. In the pipeline analysis, strain criteria are commonly adopted as failure indicators. This study defines pipeline strain-failure indicators as tensile strain exceeding 2% or compressive strain exceeding 1.4%, in accordance with the ALA–ASCE guidelines.

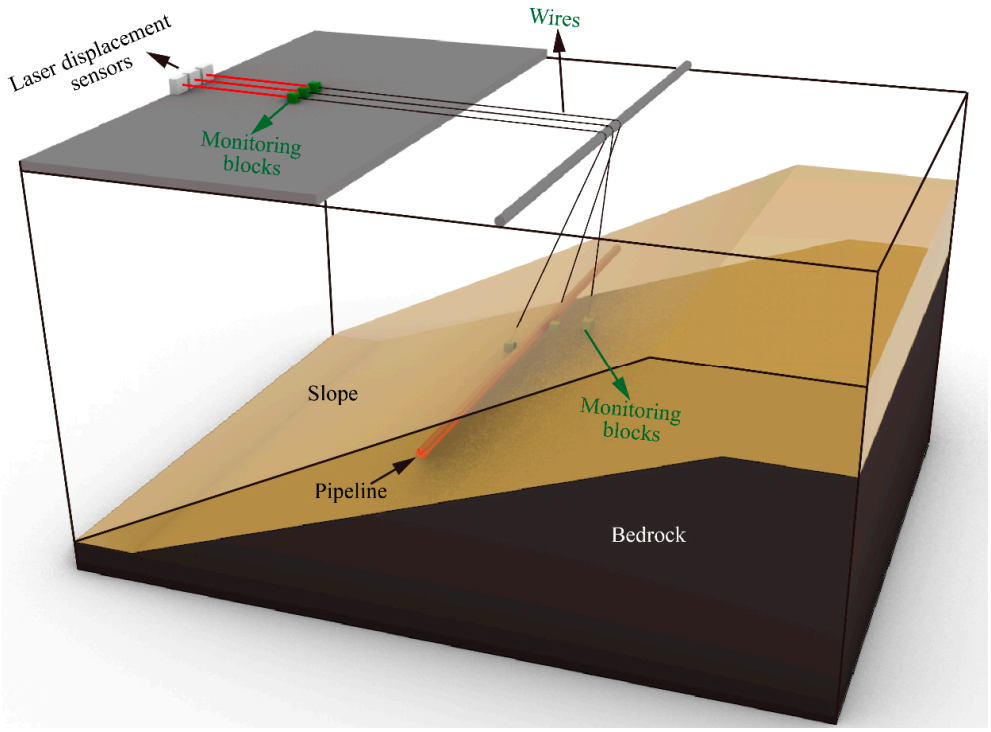

Figure 6. Schematic diagram of landslide and pipeline-displacement monitoring.

The initiation of translational landslides was simulated by applying surcharge loads at the crest of the slope, in accordance with the landslide case. The entire failure mechanism was documented using high-speed cameras. A schematic representation of the experimental setup is presented in Figure 7.

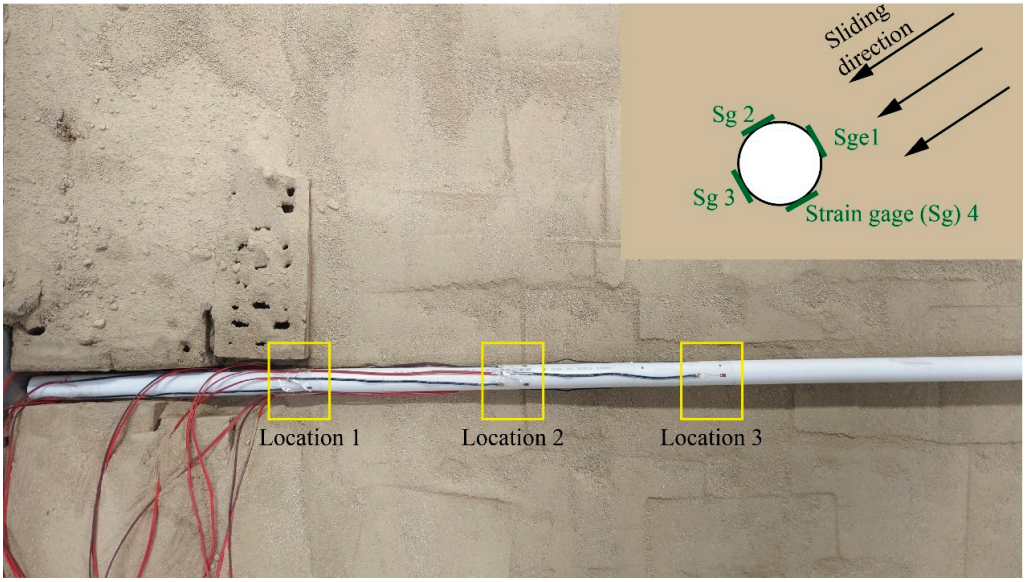

Figure 7. Setting of pipeline strain monitoring.

2.3.3. Load Application

Translational landslides were initiated by applying surcharge loading at the crest of the slope. Each increment of loading involved the placement of a 30 kg mass bag. After placing each bag, a stabilization period was observed to allow for the stabilization of landslide displacements, pipeline movements, and strains. Additional bags were then sequentially added until slope instability was observed. To maintain load stability, the mass bags were positioned on an inclined wooden board rather than being vertically stacked, thereby preventing any unintended redistribution of the load during the testing process (Figure 7).

3. Experimental Results and Discussion

3.1. Soil Response of Landslide Mass

During the experimental process, the evolution of the sliding mass is primarily characterized by two key indicators: the development of cracks and the variations in displacement. Accordingly, this section will focus on: (1) the progressive crack propagation patterns within both the sliding mass and adjacent stable regions, and (2) the displacement response characteristics of the sliding mass subjected to incremental loading conditions.

3.1.1. Development of Landslide Cracks

Figure 8 illustrates the patterns of crack propagation observed during the loading process in Experiment-L at a surcharge of 30 kg (the first loading stage) and 60 kg (the second loading stage).

Figure 8. Patterns of crack propagation during the loading process in the Experiment-L: (**a**) at a surcharge of 30 kg after 1 min and 50 s; (**b**) at a surcharge of 60 kg after 2 min and 25 s; and (**c**) at a surcharge of 60 kg after 3 min and 50 s.

The slope exhibited stable behavior throughout the first loading stage, with monitoring data confirming no signs of distress, such as surface cracking, internal displacement, or pipeline strain (Figure 8a). However, when the load increased to 60 kg, tension cracks

developed at the interface between the sliding and non-sliding regions near the crest of the slope. These cracks propagated downward, resulting in localized sliding (Figure 8b). This phenomenon aligns with the failure mechanism associated with translational landslides, where instability originates at the crest and progressively destabilizes the mid-slope and toe areas. The sliding mass experienced rapid stabilization due to the redistribution of stress, affecting only a minor volume of soil.

Figure 9 presents patterns of crack propagation observed during the loading process in Experiment-L at a surcharge of 90 kg (the third loading stage). During the third loading stage, global slope instability phenomena were observed. The upper sliding mass exerted pressure on the lower section, resulting in cracks that extended entirely through the slope. Compared to earlier stages, this phase exhibited significantly larger volumes of sliding material and an increased thickness of the sliding mass. The accumulation of displaced soil at the base of the slope ultimately led to the cessation of landslide movement.

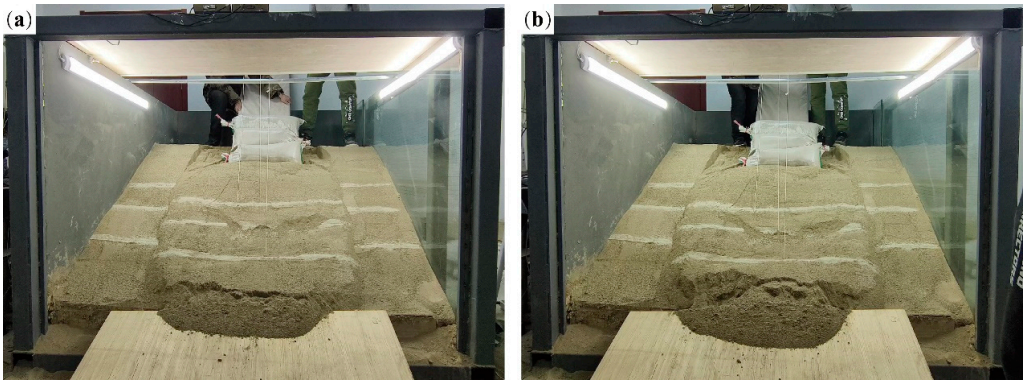

Figure 9. Patterns of crack propagation during the loading process in the Experiment-L: (**a**) at a surcharge of 90 kg after 4 min and 5 s; (**b**) at a surcharge of 90 kg after 5 min and 5 s.

Figures 10 and 11 depict the progression of cracks within the pipeline–slope system in the Experiment-LP at surcharges of 30 kg and 60 kg. Both the slope and the pipeline exhibited stability at a surcharge of 30 kg, as shown in Figure 10a. However, at a surcharge of 60 kg, initial cracks were observed at the interface between the sliding and non-sliding regions (Figure 10b), with minimal propagation toward the slope face, as depicted in Figure 11. Although transient sliding was observed initially, the system rapidly stabilized, leading to significantly shorter crack lengths compared to scenarios without the pipeline. This result confirms that the pipeline can improve the stability of the landslide.

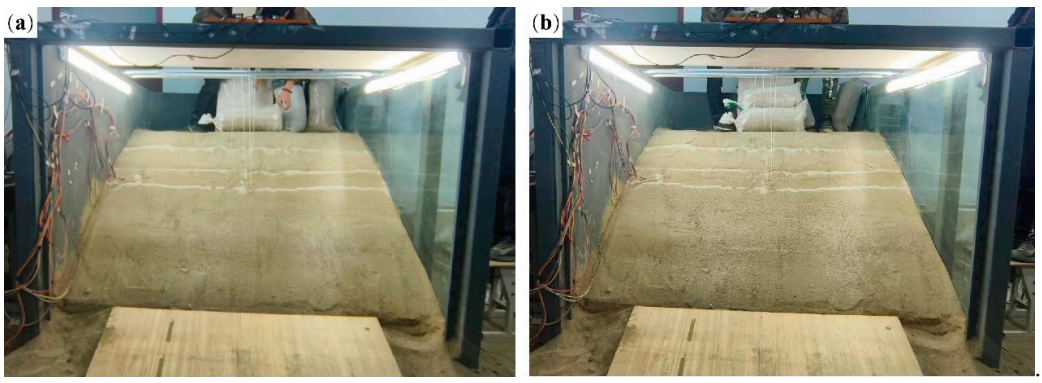

Figure 10. Patterns of crack propagation during the loading process in the Experiment-LP: (**a**) at a surcharge of 30 kg after 1 min and 25 s; (**b**) at a surcharge of 60 kg after 3 min and 55 s.

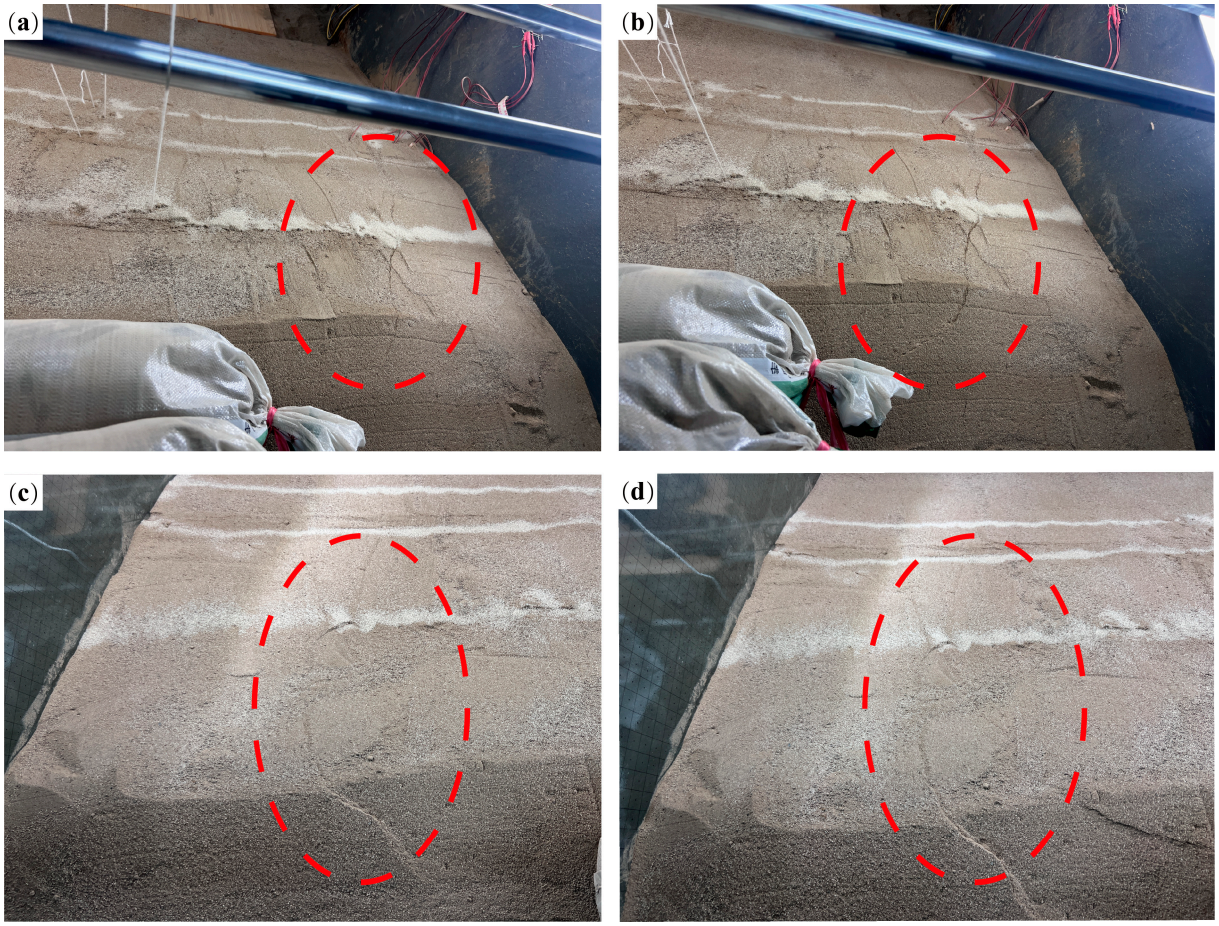

Figure 11. The crack of landslide in the Experiment-LP at a surcharge of 60 kg: (**a**) the right side after 1 min and 25 s; (**b**) the right side after 3 min and 55 s; (**c**) the left side after 1 min and 25 s; (**d**) the left side after 3 min and 55 s.

Figure 12 illustrates the development of deformation and cracks in the landslide in the Experiment-LP at a surcharge of 90 kg. During this loading stage, significant deformation was observed, characterized by notable cracks and shear displacements at the crest. The downward compression of the overlying soil imposed critical compressive and bending stresses on the pipeline, exceeding the ultimate bearing capacity of the pipeline, and leading to its fracture. Additionally, soil accumulated above the pipeline and at the landslide toe, effectively preventing any further sliding.

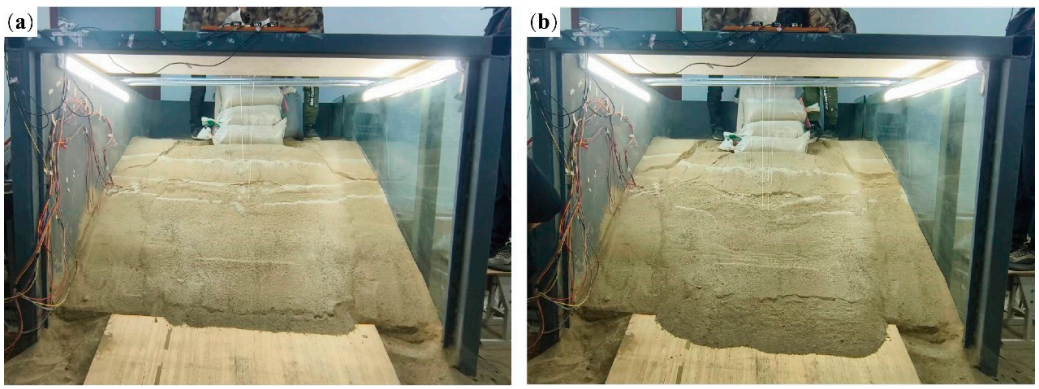

Figure 12. Patterns of crack propagation during the loading process in the Experiment-LP: (**a**) at a surcharge of 90 kg after 4 min and 5 s; (**b**) at a surcharge of 90 kg after 5 min and 25 s.

In the early phase of the third loading stage, significant sliding occurred along pre-existing fissures. Compared to the landslide that occurred in the absence of a pipeline, the observed sliding displacements were notably smaller, while soil accumulation above the pipeline became more pronounced (Figure 12a,b). The pipeline initially provided effective resistance to slope movement. However, upon fracture, this restraining capacity was lost, triggering large-scale sliding across the entire landslide area. It is noteworthy that the pre-fracture soil accumulation above the pipeline, combined with subsequent compaction during sliding, progressively decelerated the landslide movement until complete stabilization was achieved. This phenomenon suggests that the pipeline's structural integrity enables improvements in slope stability; its presence may also influence the failure mechanism and post-failure behavior of landslides.

3.1.2. Mechanisms of Landslide Movement

The surface displacement of slopes without pipelines and those with embedded pipelines are compared in Figure 13 at a surcharge of 60 kg. In the Experiment-L, the surface displacements of the upper (Line U), middle (Line M), and lower parts (Line L) of the sliding mass are 22, 15, and 16 mm, respectively. In the Experiment-LP, the surface displacements for the same sliding mass are 7, 5, and 5 mm, respectively. The upper part of the sliding mass exhibited larger displacements compared to the middle and lower parts of the sliding mass. In addition, slopes without pipelines developed significantly larger displacements, characterized by overall sliding from the crest to the toe. In contrast, slopes with embedded pipelines maintained a relatively stable condition, thereby confirming the sliding resistance of the pipeline.

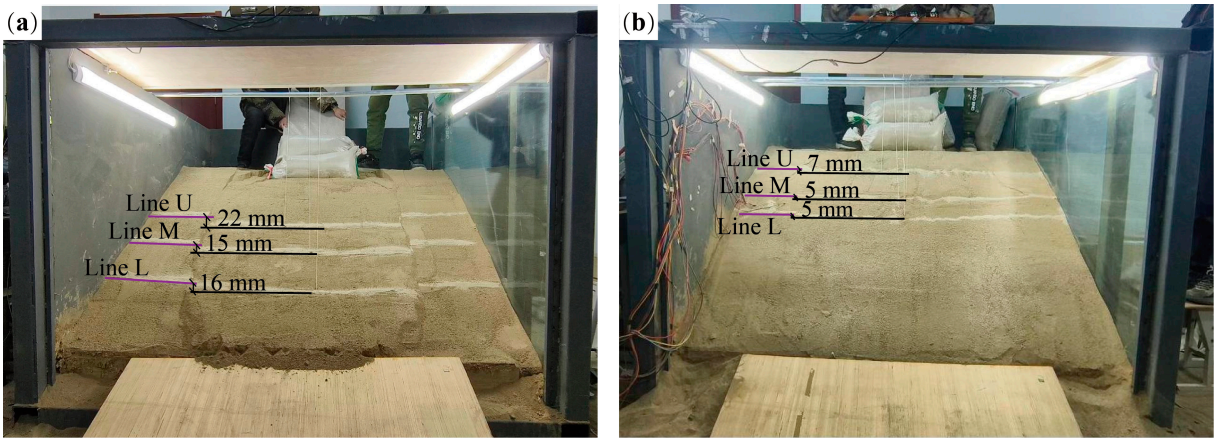

Figure 13. Displacement of the slope surface at the surcharge of 60 kg: (**a**) in the Experiment-L; (**b**) in the Experiment-LP.

The surface displacements of a slope without pipelines at a surcharge of 90 kg are presented in Figure 14. The surface displacements of the upper (Line U), middle (Line M), and lower parts (Line L) of the sliding mass are 324, 267, and 210 mm at the end of the experiment, respectively. The anti-sliding effect of the pipeline causes soil to accumulate above the pipeline. The accumulation of soil reached its maximum near the center of the landslide, with a noticeable decrease in thickness as one moves toward the lateral regions, as shown in Figure 14. The displacement time history of the slope without pipelines (Figure 15) indicates that the upper part of the landslide experienced greater displacements compared to the lower part. This observed accumulation can be attributed to the lateral movement of soil into non-sliding regions during the sliding event, coupled with a greater volume of mobilized soil in the area subjected to central loading, which ultimately resulted in an arc-shaped deposition morphology.

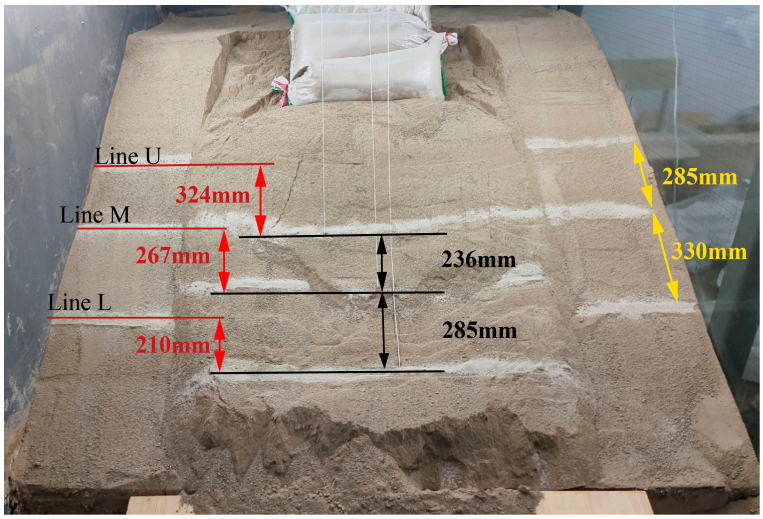

Figure 14. Displacement of the slope surface at the surcharge of 90 kg in the Experiment-L.

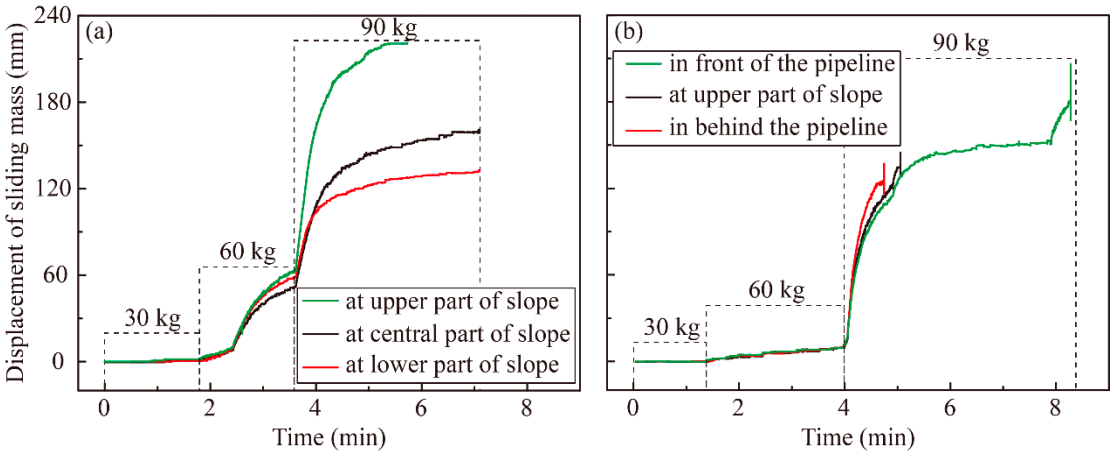

Figure 15. Displacement time histories of slope mass: (**a**) in the Experiment-L; (**b**) in the Experiment-LP.

In the slope test without pipelines (refer to Figure 14), at a surcharge of 60 kg (5–6.6 min), resulted in greater displacements in the upper slope compared to the mid and toe regions. At a surcharge of 90 kg, displacements in the upper slope increased significantly and occurred prior to movements in the mid and toe areas. This observation is consistent with the translational landslide mechanism, which is influenced by thrust originating from the crest.

The displacement time history of the slope in Experiment-L and Experiment-LP are compared in Figure 15. In the slope test conducted within the pipeline, negligible displacements were recorded during both the initial and secondary loading phases (lasting less than 4 min), indicating that the slope maintained a state of stability at a surcharge of 60 kg. Upon reaching the third loading stage, a significant landslide event was initiated, resulting in a sliding phase. The landslide persisted for a duration of approximately 4 to 5 min, during which soil displacement at three designated locations measured around 130 mm. Furthermore, it was observed that the displacement at the lower section of the pipeline exceeded that of both the upper section of the slope and the upper portion of the pipeline. This observation confirms that the presence of the pipeline obstructed the downward progression of the landslide. Following the pipeline rupture, the overlying soil mass, which had previously stabilized above the pipeline, became destabilized and initiated gradual downslope movement. This process ultimately led to a measurable increase in soil

displacement after an initial period of stabilization, demonstrating the sliding resistance effect of the pipeline prior to failure.

3.2. Pipeline Response

3.2.1. The Deformation of Pipeline

Figure 16 illustrates the pipeline fracture condition revealed during post-experimental excavation following stabilization of the landslide. While surface observations initially indicated successful sliding resistance through substantial soil deposition above the pipeline, subsequent excavation exposed critical mid-slide fractures. These structural failures resulted from translational landslide forces acting along the failure plane, demonstrating that while the pipeline exhibited sufficient shear resistance to prevent complete displacement, it ultimately succumbed to bending stresses induced by differential ground movement.

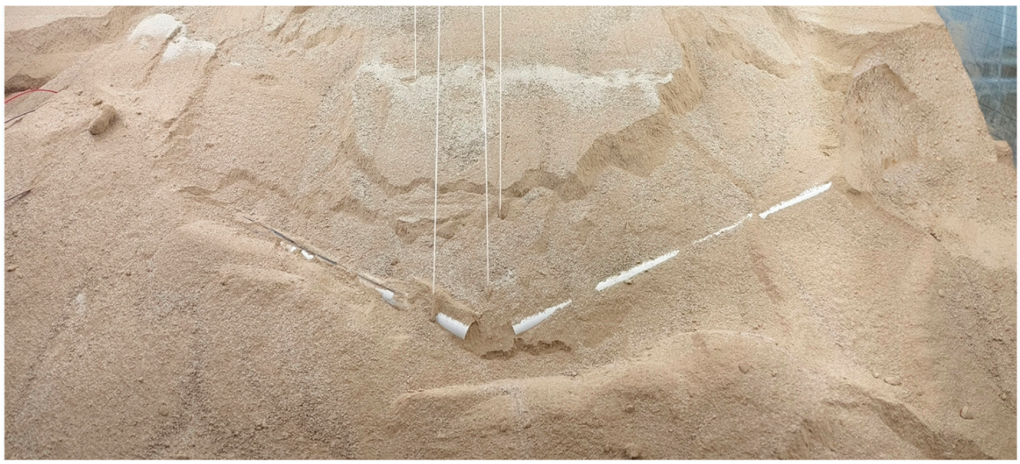

Figure 16. Fracture of the pipeline in the Experiment-LP.

3.2.2. The Strain of Pipeline

Figure 17 illustrates the strain time history of the pipeline at three different locations: the midpoint of the sliding mass, the interface between the sliding and non-sliding regions, and an intermediate position between these two points. In the first stage of the loading process (30 kg), minimal strain was recorded across all measurement positions. This result indicated that the slope maintains stability with creep displacement below instrument detection thresholds. In the subsequent stage (60 kg), a distinct differential strain distribution pattern was observed. The maximum strain was recorded at the interface between the sliding and non-sliding regions, exceeding the values noted at other locations. The magnitude of strain diminished with increasing distance from this interface. The elliptical deformation was predominant at the mid-sliding mass, and the bending deformation was small. The bending-induced tensile and compressive strains were more pronounced at the interface between the sliding and non-sliding regions. Notably, compressive strains were detected at positions 1 and 2, while symmetrical tensile strains were present at positions 3 and 4 during the first two loading stages, suggesting that bending occurred primarily in the direction of sliding. At a surcharge of 90 kg, there was a significant increase in strain of the pipeline at the midpoint of the sliding mass, exceeding the ultimate strain capacity of the pipeline and leading to fracture, as illustrated in Figure 17c. The reason for the pipeline rupture occurring at the midpoint of the sliding mass is that the pipeline in the non-sliding area is constrained, which leads to a certain degree of resistance near the non-sliding area, hindering the sliding of the slope. At the midpoint of the sliding mass, the influence of the constraint on the pipeline is minimal. Therefore, the pipeline undergoes significant deformation subjected to a larger load, which ultimately leads to the rupture of

the pipe. In addition, following the fracture, the redistribution of strain revealed modified deformation patterns.

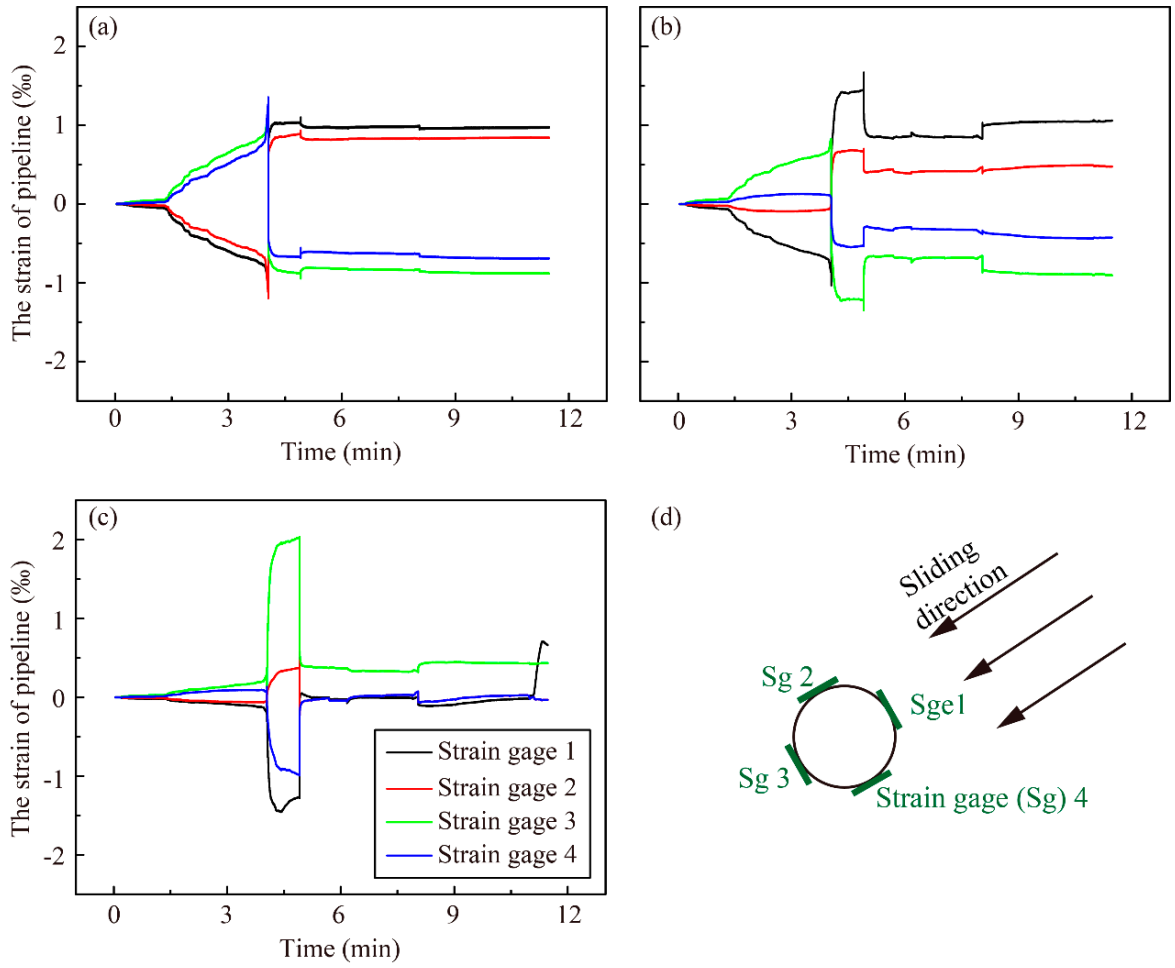

Figure 17. Strain time histories of pipeline in the Experiment-LP at: (**a**) the interface between sliding and non-sliding regions; (**b**) the quarter position of the slide mass; (**c**) the midpoint of the sliding mass; (**d**) the correlation between the positioning of the strain gauge and the sliding direction.

3.3. Discussion of Pipeline–Soil Interaction

The interaction between pipelines and sliding masses involves two principal dimensions. Firstly, pipelines have a significant influence on slope stability and the evolution of landslide movement patterns. A pipeline that traverses a slope laterally served as a flexible beam, constrained by non-sliding regions, which effectively mitigates slope creep and increases the load threshold necessary for triggering instability, thereby contributing to enhanced slope stability (Figure 18a). During an instability event, the pipeline changes the evolution of landslide movement patterns by: (1) decreasing overall sliding displacements across the upper, middle, and lower sections of the sliding mass; (2) altering patterns of soil accumulation, leading to a concentration of deposition in proximity to the pipeline; and (3) redirecting the movement of internal soil particles. Under the influence of gravitational and thrust forces, soil particles navigate around the pipeline in a circumferential manner, resulting in their accumulation beneath the depth at which the pipeline is buried.

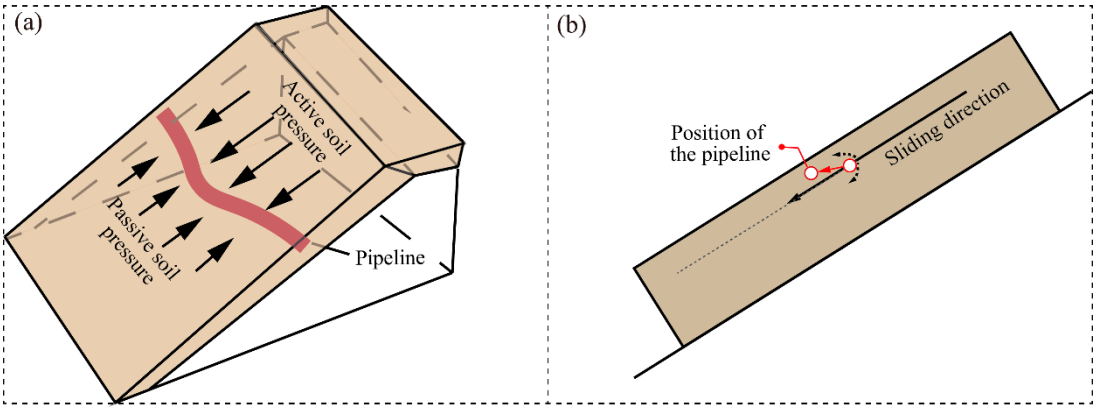

Figure 18. Pipeline–soil interaction in the landslide: (**a**) pipeline–soil interaction force; (**b**) pipeline movement direction.

In contrast, the sliding masses have significant impacts on pipelines. During a sliding event, the pipeline situated within the sliding mass is subjected to thrust forces, which result in considerable deformation. The peak strain of pipelines is observed at the midpoint of the sliding mass due to the thrust generated by the landslide, while increased strain at the interface between the sliding and non-sliding regions is attributed to shear stresses. The strains of the pipeline increase with increased sliding displacement of the sliding mass, ultimately leading to fracture when the strain of the pipeline reaches the material's strength limits. Furthermore, the accumulation of soil beneath the pipeline creates upward vertical forces that are perpendicular to the sliding plane, thereby decreasing the burial depth of pipelines (Figure 18b).

4. Conclusions

This research studied the interaction mechanisms between laterally traversing pipelines and sliding masses in translational landslides by conducting large-scale indoor model experiments. The comparative analysis provided valuable insights into the interactions between pipelines and sliding masses, focusing on the displacement and crack development in both pipeline-free and pipeline-embedded landslides, as well as the displacement and strain characteristics of the pipelines. The principal findings are summarized as follows:

(1) The crack in the slope initially develops at the crest when subjected to a top load, which is subsequently followed by downward sliding. The upper sliding mass exerts a thrust on the lower stable soil, leading to the propagation of cracks toward the toe of the slope. Once a critical loading threshold is reached, the lower slope becomes destabilized due to the thrust from the upper mass, resulting in global sliding and eventual slope failure.

(2) Pipelines that traverse the sliding mass are subjected to thrust loads in the direction of sliding, which results in peak strain of pipelines occurring at the midpoint of the sliding mass. This location is identified as the most susceptible to fracture of pipelines. Furthermore, shear forces at the interface between the sliding and non-sliding regions contribute to significant strain in these areas.

(3) When constrained by non-sliding regions, laterally embedded pipelines behave similarly to beam structures, providing resistance against thrust, shear, and bending moments. This structural behavior increases the load threshold for slope instability, thereby enhancing the overall stability of the slope.

(4) The presence of pipelines alters the evolution of landslide movement patterns. The pipeline decreases the overall sliding displacements of the sliding mass and changes

the sliding direction of the sliding mass. The movements of the sliding mass divide into upward and downward movements around the pipeline. The downward movements around the pipeline exert upward pressure on the pipeline, effectively reducing its burial depth of pipeline.

The results indicate that it is essential to avoid routing pipelines through landslide-prone areas. It is safer to lay the pipeline at the top of the slope rather than at the foot of the slope. Additionally, soil-displacement monitoring should be established on the slope to provide early warnings based on the displacement of the sliding mass. To gain a comprehensive understanding of the pipeline–soil interaction, upcoming scientific studies will concentrate on the research of microstructural parameters. The discrete-element method could be an appropriate approach for the research topics in these future studies.

Author Contributions: Conceptualization, J.Z.; methodology, J.Z.; investigation, T.X., L.L., G.S. and J.Z.; validation, J.Z.; data curation, T.X., L.L., and M.D.; writing—original draft preparation, T.X., L.L., and J.Z.; writing—review and editing, J.Z., X.L.; supervision, J.Z. All authors have read and agreed to the published version of the manuscript.

Funding: This research was funded by several funding sources, including the Research Foundation of China University of Petroleum-Beijing at Karamay (grant number XQZX20220007), the Natural Science Foundation of Xinjiang Uygur Autonomous Region (grant number 2022D01F38), the "Tianchi Talent" Introduction Plan (grant number 2021592120), the Xinjiang Tianshan Innovation Team for Research and Application of High-Efficiency Oil and Gas Pipeline Transportation Technology (grant number 2022TSYCTD0002).

Institutional Review Board Statement: Not applicable.

Informed Consent Statement: Not applicable.

Data Availability Statement: Data are available upon reasonable request.

Conflicts of Interest: The authors declare no conflicts of interest.

References

1. Huang, W.H. The development of oil and gas storage and transportation technology in China. *Oil Gas Storage Transp.* **2012**, *31*, 411–415.
2. Peng, S.B.; Liao, W.; Liu, E.B. Pipe–soil interaction under the rainfall-induced instability of slope based on soil strength reduction method. *Energy Rep.* **2020**, *6*, 1865–1875. [CrossRef]
3. Yan, Y.; Xiong, G.L.; Zhou, J.J.; Wang, R.; Huang, W.; Yang, M.; Wang, R.C.; Geng, D. A Whole Process Risk Management System for the Monitoring and Early Warning of Slope Hazards Affecting Gas and Oil Pipelines. *Front. Earth Sci.* **2022**, *9*, 812527. [CrossRef]
4. Fa-You, A.; Chen, T.H.; Yang, C.; Wu, Y.F.; Yan, S.Q. Study on Disaster Mechanism of Oil and Gas Pipeline Oblique Crossing Landslide. *Sustainability* **2023**, *15*, 3012. [CrossRef]
5. Cruz, A.M.; Krausmann, E. Vulnerability of the oil and gas sector to climate change and extreme weather events. *Clim. Chang.* **2013**, *121*, 41–53. [CrossRef]
6. Xiao, J.Z.; Kong, W.C.; Wang, X.L.; Li, M. Numerical modeling and assessment of natural gas pipeline separation in China: The data from Henan Province. *Pet. Sci.* **2020**, *17*, 268–278. [CrossRef]
7. Huang, W.H.; Chen, J.D.; Fu, C.; Huang, Y. Approach for natural gas to be a primary energy source in China. *Front. Eng. Manag.* **2019**, *6*, 467–476. [CrossRef]
8. Niu, H.T. Smart safety early warning model of landslide geological hazard based on BP neural network. *Saf. Sci.* **2020**, *123*, 104572.
9. Zahid, U.; Godio, A.; Mauro, S. An analytical procedure for modelling pipeline landslide interaction in gas pipelines. *J. Nat. Gas Sci. Eng.* **2020**, *81*, 103474. [CrossRef]
10. Zhang, J.; Liang, B.F.; Pan, B.; Shen, K.R.; Chen, L.Y. Mechanical Response Analysis of Gas Pipeline under Traction Landslide. *Press. Vessel Technol.* **2020**, *37*, 19–25+38+58.
11. Zhang, H.; Liu, X.B. Design strain calculation model for oil and gas pipelines subject to geological hazards. *Oil Gas Storage Transp.* **2017**, *36*, 91–97.

12. Lin, D.; Lei, Y.; Xu, K.; Huang, R. An experiment on the effect of a transverse landslide on pipelines. *Acta Pet. Sin.* **2011**, *32*, 728–732.
13. Feng, W.K.; Huang, R.Q.; Liu, J.T.; Xu, X.; Luo, M. Large-scale field trial to explore landslide and pipeline interaction. *Soils Found.* **2015**, *55*, 1466–1473. [CrossRef]
14. Calvetti, F.; Prisco, C.; Nova, R. Experimental and Numerical Analysis of Soil–Pipe Interaction. *J. Geotech. Geoenviron. Eng.* **2004**, *130*, 1292–1299. [CrossRef]
15. Lian, J.Q.; Shi, R.; Fan, R.D.; Li, X. Study on the Pipe–soil Interaction under Instability of Slope Based on Flume Experiment. *J. Phys. Conf. Ser.* **2022**, *2381*, 012060. [CrossRef]
16. Guan, W.; Wu, H.G.; Wu, D.Y.; Tang, L.; Wei, H. Study on Interaction Mechanism of Natural Gas Pipe-Landslide System Reinforced by Micropile Groups Based on Model Test. *Geofluids* **2022**, *2022*, 8436297. [CrossRef]
17. Katebi, M.; Wijewickreme, D.; Maghoul, P.; Roy, K. Lateral force-displacement response of buried pipes in slopes. *Géotechnique* **2023**, *73*, 375–387. [CrossRef]
18. Daiyan, N.; Kenny, S.; Phillips, R.; Popescu, R. Investigating pipeline–soil interaction under axial–lateral relative movements in sand. *Can. Geotech. J.* **2011**, *48*, 1683–1695. [CrossRef]
19. Zhang, W.Y.; Askarinejad, A. Behaviour of buried pipes in unstable sandy slopes. *Landslides* **2019**, *16*, 283–293. [CrossRef]
20. He, W.G.; Li, H.Z.; Jia, L.L.; Yao, G.Z. Deformation monitoring and mechanism analysis on landslide along China-Myanmar Natural Gas Pipeline: Case of Shazi Town Landslide in west of Guizhou Province. *Yangtze River* **2020**, *51*, 138–143.
21. Jahromi, F.H.; Jafarzadeh, F.; Zakaria, S.M. Experimental study of burial depth effect on embedded pipe deformations in sandy slopes under dynamic landsliding. *Soil Dyn. Earthq. Eng.* **2018**, *114*, 281–297. [CrossRef]
22. Wang, D.Y. Study on Improvement of Pipe-Soil Spring Model in Mountain Slope Area. *J. Phys. Conf. Ser.* **2022**, *2381*, 012090. [CrossRef]
23. Jiang, K.; Wang, D.; Yu, Z.F.; Huang, D. Analysis of Pipeline Damage Caused by Lateral Landslides: Taking Two Explosion Accidentsin the Qinglong Section of China-Myanmar Pipeline in Guizhou as an Example. *Sci. Technol. Eng.* **2023**, *23*, 8988–8995.